Relativistic Positioning Systems in Flat Space-Time with Inertial, Hyperbolic and Rotating Emitters

Ramón Serrano Montesinos * and Juan Antonio Morales-Lladosa

Posted Date: 9 April 2026

doi: 10.20944/preprints202604.0665.v1

Keywords: relativistic positioning systems; examples; inertial; hyperbolic; rotating emitters; configuration regions; solution

 doi:10.20944/preprints202604.0665.v1

Article

Relativistic Positioning Systems in Flat Space-Time with Inertial, Hyperbolic and Rotating Emitters

Ramón Serrano Montesinos [1,*] and Juan Antonio Morales-Lladosa [1,2]

[1] Departament d'Astronomia i Astrofísica, Universitat de València, 46100 Burjassot, València, Spain
[2] Observatori Astronòmic, Universitat de València, 46980 Paterna, València, Spain
* Correspondence: rasemon@alumni.uv.es

Abstract

We analyse different configurations of four emitters in a Relativistic Positioning System (RPS) with: (i) one inertial and three static emitters, (ii) one hyperbolic and three static emitters and (iii) three rotating and one static emitter. For every configuration we analyse the emission/reception conditions, represent the emission configuration regions and write the user's location solution. We follow the notions and terminology of previous works in this topic.

Keywords: relativistic positioning systems; examples; inertial; hyperbolic; rotating emitters; configuration regions; solution

1. Introduction

A Relativistic Positioning System (RPS) is essentially a set of four clocks broadcasting their time by means of electromagnetic signals. Although the time of every clock may be any one, for simplicity we suppose they broadcast their *proper* times. The set of such four times imprinted on the signals converging at every space-time event constitutes a (four-dimensional) physical coordinate system for the region reached by the signals. Such coordinates are called *emission coordinates* [1]. Analogous Newtonian emission coordinate systems have been constructed from sonic signals and classified in [2].

In this work we are mainly concerned with specific RPSs in Minkowski space-time. The affine geometry and light cone structure of flat space-time make viable analytical constructions of RPSs with both inertial and non-inertial emitters. At first glance, these constructions may seem somewhat academic for practical purposes. However, concrete RPS examples contribute to develop current RPS theory and future applications. Furthermore, the study of Minkowskian RPSs pave the way for realistic constructions in a known gravitational field, modelled as a curved Lorentzian geometry, in which the use of the Ruse-Synge world function for the null geodesics [3,4] or the application of distance geometry concepts [5,6] may result mandatory.

The main aim of RPS theory is to give a precise physical frame for the location of events in a gravitationally unknown region in order to make relativistic gravimetry, as has been explained in [6–8]. The starting ideas of the theory of RPSs are that, in such an unknown region, the first object to be constructed is a physical coordinate system allowing to identify its events with the points of the mathematical models in use; that such physical coordinate system has to be constructed generically by means of electromagnetic signals and with a protocol independent of the particular space-time; and that the over-determined interlacement of these signals contains important information (chronometry in arbitrary directions) on the relativistic gravitational field in which we are immersed.

In [9] we have analysed the most elemental example of a RPS construction: four static emitters in flat space-time. In the present work, this construction is extended to RPSs including inertial, accelerated and rotating emitters. These constructions present significant novelties and differences with respect to the static situation, and may provide insights on fictitious gravitational potentials attached to non-inertial effects.

 doi:10.20944/preprints202604.0665.v1

The location problem in Minkowski space-time has been dealt with in [9–12]. Developments on the subject are found in [13–17], including numerical treatment and prospects. Refs. [18–20] offer relevant notions to develop the RPS theory, presenting examples in two-dimensional Lorentzian spaces. General concepts and results in 3D and 4D were communicated in [21].

In this work we develop RPS examples in Minkowski space-time with four emitters following different motions. In all cases considered we carry out the same procedure. The satellite trajectories in space-time are written and the emission/reception conditions are stated, the satellite trajectories on the grid of emission coordinates are determined and the RPS solution is interpreted by representing the characteristic regions and working out a simplified positioning example. We have used the software Mathematica to represent the characteristic regions of the RPS solutions and perform numerical calculations.

This article is organized as follows: The terminology of a RPS is introduced in section 2. Section 3 starts with a positioning example involving one inertial and three static emitters, Section 4 considers a RPS with one hyperbolic and three static emitters, Section 5 analyses the example of one static and three uniformly rotating emitters. A brief summary and conclusions are presented in Section 6. Appendix A summarizes the notation used.

2. RPS Terminology and Summary of Results in Flat Space-Time

Following [10,11], we present here a compendium of the essential RPS terminology and results used to develop this work in Minkowski space-time.

Relativistic positioning system: set of four emitters A ($A = 1,2,3,4$), of world-lines $\gamma_A(\tau^A)$, broadcasting their respective proper times τ^A by means of electromagnetic signals.

Emission coordinates of an event: the four times $\{\tau^A\}$ which are received at each space-time event x reached by the emitted signals.

Grid of a RPS: The four space $\mathcal{T} \equiv [\tau^1] \times [\tau^2] \times [\tau^3] \times [\tau^4] \approx \mathbb{R}^4$.

Configuration of the emitters for an event x: set of four events $\{\gamma_A(\tau^A)\}$ of the emitters at the emission times $\{\tau^A\}$ received at x.

In Minkowski space-time $\gamma_A \equiv O\gamma_A(\tau^A)$ denotes the position four-vector of emitter A with respect to the origin O of an inertial coordinate system $\{x^\alpha\}$, $A = 1,2,3,4$.

Configuration vector χ: vector informing of the emitter configuration at the emission times $\{\tau^A\}$ received at x,

$$\chi = *(e_1 \wedge e_2 \wedge e_3), \tag{1}$$

with $e_a = \gamma_a - \gamma_4$ ($a = 1,2,3$) the relative positions of emitters 1, 2 and 3 with respect to emitter 4, and where $*$ stands for the Hodge dual operator and $\wedge$ is the exterior product (see Appendix A for transcription into index notation). An emitter configuration is *regular* iff $\chi \neq 0$.

Null propagation equations: The following system of non-linear equations:

$$(x - \gamma_A)^2 = 0, \quad A = 1,2,3,4, \tag{2}$$

with x the user position four-vector with respect to O. The solution to these equations is the coordinate transformation from emission to inertial coordinates $x^\alpha(\tau^A)$.

Shadow of emitter A to emitter B: Space-time events x for which the future-directed null vectors $m_A = x - \gamma_A$ and $m_B = x - \gamma_B$ become collinear, $m_A \cdot m_B = 0$, lying on the future light cone with vertex at the intersection of m_A (or m_B) with γ_A.

For four emitters, there are 12 shadows in total, defining the 12 faces of the *shadow-dodecahedron* $\mathcal{D}$ in the grid of emission coordinates.

 doi:10.20944/preprints202604.0665.v1

Emission/reception conditions: conditions expressing that the null vectors $m_A = x - \gamma_A$, $A = 1,2,3,4$, are *all* either future or past oriented, $m_A \cdot m_B < 0$, $A \neq B$:

$$(e_a)^2 > 0, \quad (e_a - e_b)^2 > 0, \quad a,b = 1,2,3. \tag{3}$$

Emission region: set $\mathcal{R}$ of events reached by the four signals broadcast by the positioning system. Every $x \in \mathcal{R}$ is labelled with the corresponding emission coordinates $\{\tau^A\}$.

Characteristic emission function: map Θ that to every $x \in \mathcal{R}$ associates its emission coordinates, that is $\Theta(x) = (\tau^A)$.

Emission coordinate region: subset $\mathcal{C}$ of the emission region $\mathcal{R}$ where the gradients $d\tau^A$ are well defined and linearly independent.

Orientation of a relativistic positioning system at the event x: orientation of its emission coordinates at x or, what is the same, the orientation of the tetrad of 1-forms $\{d\tau^1, d\tau^2, d\tau^3, d\tau^4\}$. It is given by the sign $\hat{\epsilon}$ of the Jacobian determitant $j_\Theta(x)$ of Θ at x, $\hat{\epsilon} \equiv sgn\, j_\Theta(x)$. In terms of the gradients of the emission coordinates, one has

$$\hat{\epsilon} = sgn[*(d\tau^1 \wedge d\tau^2 \wedge d\tau^3 \wedge d\tau^4)]. \tag{4}$$

The orientation $\hat{\epsilon}$ of a RPS at an event x is, by definition, the orientation of its emission coordinates at x.

For regular configurations, the region where the vector χ is timelike or null, $\chi^2 \leq 0$, is called the *central region* of the RPS. In it, the orientation is uniform and is given by $\hat{\epsilon} = \text{sgn}(u \cdot \chi)$ for any observer u. But out of this region it is not possible to determine $\hat{\epsilon}$ solely from the world-lines $\gamma_A(\tau^A)$ [10], additional information is necessary [11].

Solution to the null propagation equations: The solution to (2) or, equivalently, the coordinate transformation from emission to inertial coordinates is [10]

$$x = \gamma_4 + y_* + \lambda\chi, \tag{5}$$

with y_* the particular solution, found by bringing in a subsidiary vector ξ satisfying the transversality condition $\xi \cdot \chi \neq 0$:

$$y_* = \frac{1}{\xi \cdot \chi} i(\xi) H, \tag{6}$$

where H is the configuration bivector,

$$H = \Omega_1 E^1 + \Omega_2 E^2 + \Omega_3 E^3, \tag{7}$$

with

$$E^1 = *(e_2 \wedge e_3), \quad E^2 = *(e_3 \wedge e_1), \quad E^3 = *(e_1 \wedge e_2), \tag{8}$$

and

$$\lambda = -\frac{y_*^2}{(y_* \cdot \chi) + \hat{\epsilon}\sqrt{\Delta}}, \quad \Delta = (y_* \cdot \chi)^2 - y_*^2 \chi^2. \tag{9}$$

The following example with one inertial and three static emitters is the logical extension of the example analysed in [9] involving four static emitters spatially forming an orthogonal tetrahedron. In this example, however, the inertial emitter moves along the spatial bisectrix in such a way that, at zero coordinate time, the four emitters form a regular tetrahedron.

3. RPS with One Inertial and Three Static Emitters

In this example in Minkowski space-time, we consider emitters 2, 3 and 4 static with respect to an inertial observer u ($u^2 = -1$). Emitter 1 is moving with constant velocity β with respect to u along the spatial main bisectrix, in such a way that at proper time $\tau^1 = 0$ the four emitters are spatially forming

 doi:10.20944/preprints202604.0665.v1

a regular tetrahedron of vertices $(1,1,1)$, $(1,-1,-1)$, $(-1,1,-1)$ and $(-1,-1,1)$. As $\tau^1 \to \pm\infty$, its spatial position of emitter 1 tends to $\pm\infty$ along the main bisectrix $(1,1,1)$.

3.1. Emitters' World-Lines and Emission/Reception Conditions

Thus, the world-lines referred to the inertial obeserver u are written as:[1]

$$\begin{aligned}\gamma_1 =&\gamma\tau^1\left[u+\frac{\beta}{\sqrt{3}}(1,1,1)\right]+(1,1,1), \quad \gamma_2=\tau^2\,u+(1,-1,-1),\\ \gamma_3 =&\tau^3\,u+(-1,1,-1), \qquad\qquad\qquad \gamma_4=\tau^4\,u+(-1,-1,1),\end{aligned}$$

where $\gamma=(1-\beta^2)^{-\frac{1}{2}}$. The velocity β is expressed as a fraction of the speed of light in vacuum c ($\beta<1$). We consider that the proper times of emitters 2, 3 and 4 are synchronised at their common origin $\tau^2=\tau^3=\tau^4=0$ and that the proper time of emitter 1 is synchronised with theirs at $\tau^1=0$. The distance d_1 covered by emitter 1 in one second of coordinate time $\Delta x^0=1\ s$ ($\Delta\tau^1=\gamma^{-1}\Delta x^0=\gamma^{-1}\ s$) is $d_1=\beta\ ls$. [2]

Defining[3]

$$\begin{aligned}q_1=\gamma\tau^1-\tau^4, \quad q_2=\tau^2-\tau^4, \quad q_3=\tau^3-\tau^4,\\ \Gamma(\tau^1)=\frac{\gamma\beta}{\sqrt{3}}\tau^1,\end{aligned}$$

one obtains the following position vectors with respect to the fourth emitter, $e_a=\gamma_a-\gamma_4$, $a=1,2,3$:

$$e_1=q_1\,u+(\Gamma+2,\Gamma+2,\Gamma), \quad e_2=q_2\,u+(2,0,-2), \quad e_3=q_3\,u+(0,2,-2), \tag{10}$$

and the following world-functions $\Omega_a=\frac{1}{2}(e_a)^2$, $a=1,2,3$:

$$\Omega_1=\tfrac{1}{2}(2(\Gamma+2)^2+\Gamma^2-q_1^2), \quad \Omega_2=\tfrac{1}{2}(8-q_2^2), \quad \Omega_3=\tfrac{1}{2}(8-q_3^2). \tag{11}$$

A regular emitter configuration is an emission/reception configuration (see [9,10]) iff all relative emitter positions are space-like, $e_a^2>0$ and $(e_a-e_b)^2>0$, $a,b=1,2,3$, that is, when the following emission/reception conditions are satisfied:

$$\begin{aligned}&|q_1|<\sqrt{2(\Gamma+2)^2+\Gamma^2}, \quad |q_2|<\sqrt{8}, \quad |q_3|<\sqrt{8},\\ &|q_1-q_2|<\sqrt{2(\Gamma+2)^2+\Gamma^2}, \quad |q_1-q_3|<\sqrt{2(\Gamma+2)^2+\Gamma^2}, \quad |q_2-q_3|<\sqrt{8}.\end{aligned} \tag{12}$$

Notice that the family of parabolas

$$y_\gamma(\tau^1)\equiv 2(\Gamma+2)^2+\Gamma^2=(\gamma^2-1)(\tau^1)^2+\frac{8}{\sqrt{3}}\sqrt{\gamma^2-1}\,\tau^1+8 \tag{13}$$

shares the same vertex height, which does not depend on γ, $y_\gamma(\tau_v^1)=\frac{8}{3}$, with $\tau_v^1=-\frac{4}{\sqrt{3}\gamma\beta}$.

3.2. Emitters' Trajectories on the Grid $\mathcal{T}$

The grid coordinate τ^B of the trajectory γ_A on the grid for $B\neq A$ is computed from the intersection of the past null cone of γ_A with the world-line γ_B, by solving the light-cone equation $(\gamma_A-\gamma_B)^2=0$

---

[1] For clarity, for any space-time vector living in the space orthogonal to u, $E_\perp$, we will abuse the notation and use a three dimensional vector (as in $(1,1,1)$) when, in fact, it is a four-dimensional space-time vector with vanishing first coordinate (such as $(0,1,1,1)$).

[2] For $\beta=\frac{1}{2}$, $d_1=\frac{1}{2}\ ls\approx 150.000\ km$.

[3] For convenience, we use subindexes in q_a, $a=1,2,3$, despite being defined in terms of contravariant emission coordinates. Also, when referring to a defined function (such as $\Gamma(\tau^1)$), we may omit the argument (as in $\Gamma+2$).

 doi:10.20944/preprints202604.0665.v1

for τ^B and selecting the solution that corresponds to an emission event on γ_B. The grid coordinate τ^A of the trajectory γ_A is simply τ^A. Since all four grid coordinates of the trajectory γ_A depend on τ^A, considered the parameter of the trajectory, we omit the superscript.

$$\begin{aligned}
S_1(\tau) &: \left(\tau, \gamma\tau - \sqrt{y_\gamma(\tau)}, \gamma\tau - \sqrt{y_\gamma(\tau)}, \gamma\tau - \sqrt{y_\gamma(\tau)}\right), \\
S_2(\tau) &: \left(\gamma\left[\tau + \tfrac{4\beta}{\sqrt{3}}\right] - \sqrt{z_\beta(\tau)}, \tau, \tau - \sqrt{8}, \tau - \sqrt{8}\right), \\
S_3(\tau) &: \left(\gamma\left[\tau + \tfrac{4\beta}{\sqrt{3}}\right] - \sqrt{z_\beta(\tau)}, \tau - \sqrt{8}, \tau, \tau - \sqrt{8}\right), \\
S_4(\tau) &: \left(\gamma\left[\tau + \tfrac{4\beta}{\sqrt{3}}\right] - \sqrt{z_\beta(\tau)}, \tau - \sqrt{8}, \tau - \sqrt{8}, \tau\right),
\end{aligned} \tag{14}$$

with

$$z_\beta(\tau) \equiv \gamma^2[\tau + \tfrac{4\beta}{\sqrt{3}}]^2 - \tau^2 + 8.$$

This family of parabolas shares the same discriminant with $y_\gamma(\tau)$, $\Delta_z = -\frac{32}{3}\gamma^2\beta^2 < 0$, and the same vertex height $z_\beta(\tau_v) = y_\gamma(\tau_v^1) = \frac{8}{3}$, with $\tau_v = \gamma\tau_v^1$.

The important property is that at τ_v^1 emitter 1 is at the spatial location $-\frac{1}{3}(1,1,1)$, being spatially coplanar with emitters 2, 3 and 4 and situated at the circumcenter of the triangle formed by these emitters. This property becomes relevant in Section 3.3.

In this inertial example, the emitters' trajectories on the grid are not straight lines. Then, we can rewrite trajectories (14) to compare them with the static case [9]:

$$\begin{aligned}
S_1(\tau) &: \tau(1,\gamma,\gamma,\gamma) - \sqrt{8}\sqrt{1 + \frac{\gamma\beta}{\sqrt{3}}\tau + \frac{\gamma^2\beta^2}{8}\tau^2}(0,1,1,1), \\
S_2(\tau) &: \tau(\gamma,1,1,1) - \sqrt{8}\left(\sqrt{1 - \frac{\tau^2}{8} + \frac{\gamma^2}{8}(\tau + \frac{4\beta}{\sqrt{3}})^2} + \frac{4\beta}{\sqrt{3}}, 0, 1, 1\right), \\
S_3(\tau) &: \tau(\gamma,1,1,1) - \sqrt{8}\left(\sqrt{1 - \frac{\tau^2}{8} + \frac{\gamma^2}{8}(\tau + \frac{4\beta}{\sqrt{3}})^2} + \frac{4\beta}{\sqrt{3}}, 1, 0, 1\right), \\
S_4(\tau) &: \tau(\gamma,1,1,1) - \sqrt{8}\left(\sqrt{1 - \frac{\tau^2}{8} + \frac{\gamma^2}{8}(\tau + \frac{4\beta}{\sqrt{3}})^2} + \frac{4\beta}{\sqrt{3}}, 1, 1, 0\right).
\end{aligned}$$

And approximate them up to first order in β to obtain the following straight lines:

$$\begin{aligned}
S_1(\tau) &: \tau\left(1, 1 - \sqrt{\tfrac{2}{3}}\beta, 1 - \sqrt{\tfrac{2}{3}}\beta, 1 - \sqrt{\tfrac{2}{3}}\beta\right) - (0, \sqrt{8}, \sqrt{8}, \sqrt{8}), \\
S_1(\tau) &: \tau(1,1,1,1) - \left(\sqrt{8} - \frac{4}{\sqrt{3}}\beta, 0, \sqrt{8}, \sqrt{8}\right), \\
S_1(\tau) &: \tau(1,1,1,1) - \left(\sqrt{8} - \frac{4}{\sqrt{3}}\beta, \sqrt{8}, 0, \sqrt{8}\right), \\
S_1(\tau) &: \tau(1,1,1,1) - \left(\sqrt{8} - \frac{4}{\sqrt{3}}\beta, \sqrt{8}, \sqrt{8}, 0\right),
\end{aligned}$$

in agreemeent with the results obtained for four static emitters.

3.3. Shadow-Dodecahedron

As can be seen from the emission/reception conditions (12), and also from the RPS solution below, this example with one inertial emitter moving with respect to three static emitters can not be fully described on the quotient grid $\mathcal{Q} \equiv [q_1] \times [q_2] \times [q_3] \approx \mathbb{R}^3$, essentially because of the term Γ which depends on τ^1. Instead, one can consider τ^1 a parameter and work on the grid $\mathcal{T}_1(\tau^1) \equiv [\tau^2] \times [\tau^3] \times [\tau^4] \approx \mathbb{R}^3$ for each value of τ^1. In the example with four static emitters [9],

 doi:10.20944/preprints202604.0665.v1

on an analougous $\mathcal{T}_1$-grid, the shadow-dodecahedron $\mathcal{D}$ moves along the main bisectrix for each τ^1 but its shape does not change, that is, the relative positions of its vertices remain constant for every τ^1. In the case of one moving emitter, however, apart from a translation of the shadow-dodecahedron on the $\mathcal{T}_1$-grid for each τ^1 along the main bisectrix, there is a longitudinal deformation along that axis since its 14 vertices depend on τ^1 as follows:

$$
\begin{aligned}
V_1 &= (G_+, G_+, G_+), & V_2 &= (G_-, G_-, G_-),\\
V_3 &= (G_+ - \sqrt{8}, G_+, G_+), & V_4 &= (G_+, G_+ - \sqrt{8}, G_+),\\
V_5 &= (G_+, G_+, G_+ - \sqrt{8}), & V_6 &= (G_- + \sqrt{8}, G_-, G_-),\\
V_7 &= (G_-, G_- + \sqrt{8}, G_-), & V_8 &= (G_-, G_-, G_- + \sqrt{8}),\\
V_9 &= (G_+ - \sqrt{8}, G_+ - \sqrt{8}, G_+), & V_{10} &= (G_+, G_+ - \sqrt{8}, G_+ - \sqrt{8}),\\
V_{11} &= (G_+ - \sqrt{8}, G_+, G_+ - \sqrt{8}), & V_{12} &= (G_- + \sqrt{8}, G_- + \sqrt{8}, G_-),\\
V_{13} &= (G_-, G_- + \sqrt{8}, G_- + \sqrt{8}), & V_{14} &= (G_- + \sqrt{8}, G_-, G_- + \sqrt{8}),
\end{aligned}
$$

with $G_\pm(\tau^1) \equiv \gamma\tau^1 \pm \sqrt{y_\gamma(\tau^1)}$. Of these 14 vertices, only one concides with a satellite trajectory on the grid $\mathcal{T}_1$, namely V_2 with the trajectory of satellite 1.

The dodecahedron contracts longitudinally along the main bisectrix as we approach $\tau_v^1 = -\frac{4}{\sqrt{3}\gamma\beta}$ from left and right, where it is smallest. Figure 1 shows the shadow-dodecahedron for $\beta = \frac{1}{2}$ at the endpoints and midpoint of the interval[4] $\tau^1 \in [-\frac{8}{\sqrt{3}\gamma\beta}, 0]$, that is, for $\tau^1 = -8$, $\tau^1 = -4$ and $\tau^1 = 0$. At the midpoint $\tau_v^1 = -4$ the dodecaedron is smallest.

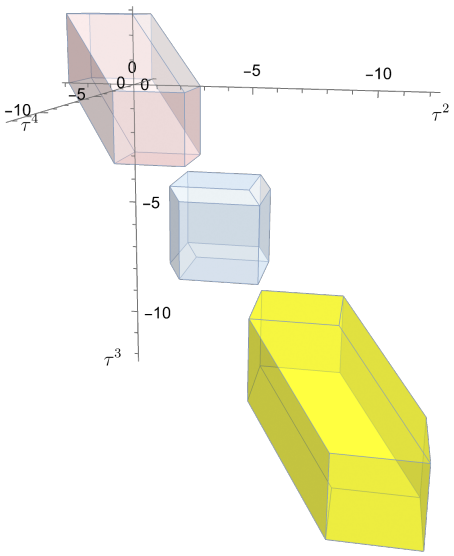

Figure 1. The shadow dodecahedron for $\beta = \frac{1}{2}$ at $\tau^1 = 0$ (purple), $\tau^1 = -4$ (blue) and $\tau^1 = -8$ (yellow)

We can study the motion of the shadow-dodecahedron along the main bisectrix through the motion of the spatial circumcenter of the tetrahedron formed by the four satellites, whose world-line γ_c, parametrized with the proper time of emitter 1 (τ^1), is expressed as:

$$
\begin{aligned}
\gamma_c &= \gamma\tau^1 u + \frac{\omega_c}{\sqrt{3}}(1,1,1), \\
\omega_c &= \frac{\beta\gamma\tau^1(6+\sqrt{3}\beta\gamma\tau^1)}{8+2\sqrt{3}\beta\gamma\tau^1}\,.
\end{aligned}
\tag{15}
$$

As said in the previous section, this world-line is degenerate at $\tau^1 = \tau_v^1$, when all four emitters are spatially coplanar.

[4] In this interval $y_\gamma(\tau^1) \leq 8$.

 doi:10.20944/preprints202604.0665.v1

We can now write the trajectory of the spatial circumcenter on the grid $\mathcal{T}_1$:

$$S_c = (f_c, f_c, f_c),$$
$$f_c(\tau^1) = \gamma\tau^1 - \frac{\sqrt{\Delta_c}}{2(3\Gamma+4)},$$
$$\Delta_c = 81\,\Gamma^4 + (36\sqrt{3}+324)\,\Gamma^3 + (120\sqrt{3}+432)\,\Gamma^2 + (96\sqrt{3}+288)\,\Gamma + 192.$$

In the $\mathcal{T}_1$-grid, the spatial circumcenter described by world-line γ_c (15) moves along the bisectrix of the grid. We can determine whether it lies inside the shadow-dodecahedron for any τ^1 by comparing its coordinates with those of vertices V_1 and V_2, the end vertices on the bisectrix. It lies inside the dodecahedron for any $\tau^1 > \tau^1_b$ and $\tau^1 < \tau^1_a$, where τ^1_a and τ^1_b are the τ^1-coordinates of the two intersection points of $y_\gamma(\tau^1)$ and $g_c(\tau^1) \equiv \frac{\Delta_c}{4(3\Gamma+4)^2}$. In the interval $[\tau^1_a, \tau^1_b]$ the function $g_c(\tau^1)$ diverges at $\tau^1 = \tau^1_v$, when the four emitters are spatially coplanar (see Section 3.2).

3.4. Interpreting the RPS Solution

We now represent the caracteristic regions of the RPS solution in Cartesian coordinates for this case, depending on the causal character of the configuration vector χ. Unlike the static situation [9], these regions change with every inertial instant x^0 for a given velocity β. But, as in the static situation, for every x^0 the RPS solution is defined in the whole Euclidean space $\{x^1, x^2, x^3\}$. Figure 2 shows these regions and the region $j_\Theta(x) = 0$, where the jacobian determinant of the transformation from inertial to emission coordinates vanishes, for $\beta = \frac{1}{2}$ and $x^0 = 1$.

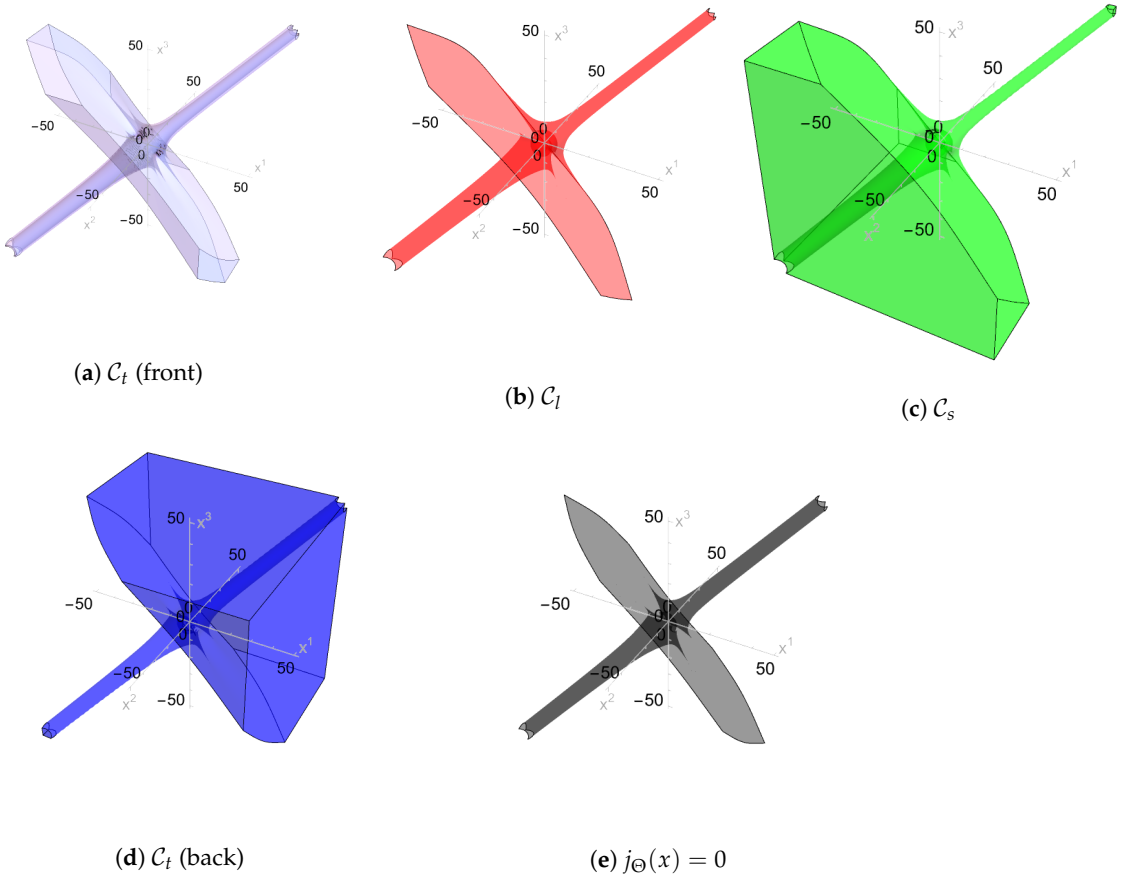

(**a**) $\mathcal{C}_t$ (front) (**b**) $\mathcal{C}_l$ (**c**) $\mathcal{C}_s$

(**d**) $\mathcal{C}_t$ (back) (**e**) $j_\Theta(x) = 0$

Figure 2. Representation of the emission configuration regions, at $x^0 = 1$, for a RPS with one inertial emitter moving with $\beta = \frac{1}{2}$ and three static emitters. The emission configuration regions $\mathcal{C}_s$ (space-like), $\mathcal{C}_l$ (light-like) and $\mathcal{C}_t$ (time-like) are colored in green, red and blue, respectively. The 3-surface where $j_\Theta(x)$ vanishes is shown in black.

 doi:10.20944/preprints202604.0665.v1

Figure 3 includes a two dimensional slice of the emission configuration regions shown in Figure 2, through the plane containing emitters 1, 2 and 4 at $x^0 = 1$ ($\beta = \frac{1}{2}$). The intersection with $j_\Theta(x) = 0$ is also represented. We can see that around the satellites the configuration regions are interlaced with each other.

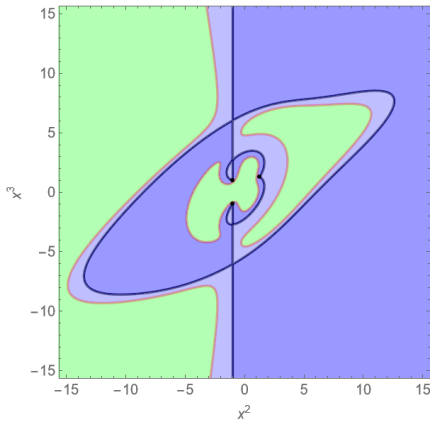

(**a**) Slice of the emission configuration regions.

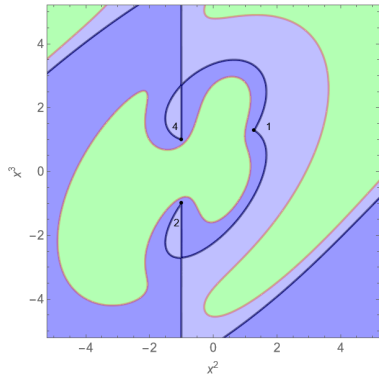

(**b**) Zoom in of the region containing satellites 1, 2 and 4.

Figure 3. Slice of the emission configuration regions (shown in Figure 2) through the plane containing emitters 1, 2 and 4 at $x^0 = 1$ ($\beta = \frac{1}{2}$). Black points represent satellites as indicated.

To remark the essential properties of the RPS solution in this example, we consider the inertial coordinate location of those users whose emission coordinates satisfy the restrictions $\tau^1 = -\sigma, \tau^2 = \tau^3 = \tau^4 = \sigma$. We start by computing the configuration covector (1) using (10):

$$\chi_\mu = -4\Big(\sqrt{3}\gamma\beta\sigma - 4, (1+\gamma)\sigma, (1+\gamma)\sigma, (1+\gamma)\sigma\Big). \tag{16}$$

To calculate the particular solution y_*, we first compute the configuration bivector H using (10), (11), (8) and (7). Choosing the transversal vector $\xi = u$, Equation (6) then yields:

$$y_{*_\mu} = \frac{4}{D}\Big(0, \sigma^2(1+\gamma) + 2\sqrt{3}\gamma\beta\sigma - 4, \sigma^2(1+\gamma) + 2\sqrt{3}\gamma\beta\sigma - 4, \sigma^2(1+\gamma) + 4\Big), \tag{17}$$

with $D = 4(\sqrt{3}\gamma\beta\sigma - 4)$. With this choice of ξ, the transversality condition restricts this solution to $\{\sigma \in \mathbb{R} | \sigma \neq -\tau_v^1 = \frac{4}{\sqrt{3}\gamma\beta}\}$. As said earlier, at $\tau^1 = \tau_v^1$ all four emitters are spatially coplanar, leading to a degenerate situation.[5]

The solution (5) reads:

$$x^\mu(-\sigma, \sigma, \sigma, \sigma) = (\sigma, -1, -1, 1) + y_* - \frac{\lambda_1}{\lambda_2}\chi, \tag{18}$$

with polynomial functions of σ

$$\begin{aligned}
\lambda_1 &= 4\Big(3(1+\gamma)^2\sigma^4 + 8\sqrt{3}\gamma\beta(1+\gamma)\sigma^3 + 8(3\gamma^2 - \gamma - 4)\sigma^2 - 32\sqrt{3}\gamma\beta\sigma + 48\Big),\\
\lambda_2 &= D\Big(-12(1+\gamma)^2\sigma^3 - 16\sqrt{3}\gamma\beta(1+\gamma)\sigma^2 + 16(1+\gamma)\sigma + \hat{\epsilon}D\sqrt{\Delta_\sigma}\Big),\\
\Delta_\sigma &= \frac{\lambda_1}{4} - 8(1+\gamma)^2\sigma^2.
\end{aligned}$$

[5] At $\tau^1 = \tau_v^1, \tau^2 = \tau^3 = \tau^4 = -\tau_v^1$, the vector $\xi = u$ is not transversal but orthogonal to the configuration.

 doi:10.20944/preprints202604.0665.v1

In this case, $q_1 = -\sigma(\gamma+1)$, $q_2 = q_3 = 0$, and the emission-reception conditions (12) are reduced to:

$$|\sigma| < \frac{1}{\gamma+1}\sqrt{(\gamma^2-1)\sigma^2 - \frac{8\gamma\beta}{\sqrt{3}}\sigma + 8}\,, \tag{19}$$

where we have taken into account (13) and which is equivalently written as

$$P(\sigma) \equiv \sigma^2 + \frac{4}{\sqrt{3}}\sqrt{\frac{\gamma-1}{\gamma+1}}\,\sigma - \frac{4}{\gamma+1} < 0. \tag{20}$$

The roots of $P(\sigma) = 0$,

$$\sigma_\pm = \frac{2}{\sqrt{3}}\frac{1}{\sqrt{\gamma+1}}\left(-\sqrt{\gamma-1} \pm \sqrt{\gamma+2}\right), \tag{21}$$

provide the limiting values for σ imposed by the emission-reception conditions.

Table 1 shows the result setting $\beta = \frac{1}{2}$ for different values of σ. In this particular case, the emission-reception condition (19) imposes

$$-1.71 \approx \frac{2}{3}(-2\sqrt{3} - \sqrt{6(\sqrt{3}-1)}+3) < \sigma < \frac{2}{3}(-2\sqrt{3} + \sqrt{6(\sqrt{3}-1)}+3) \approx 1.09.$$

(i) For $\sigma = \frac{1}{2}$, the emitter configuration is space-like at
$x^\mu = \frac{1}{44}\left(9\left(5\sqrt{3}+3\right), -\left(9\sqrt{3}+23\right), -\left(9\sqrt{3}+23\right), -\left(9\sqrt{3}+23\right)\right)$, which is the sole emission solution (with $\hat{\epsilon} = -1$). The solution with $\hat{\epsilon} = 1$ is a reception solution.

(ii) For $\sigma = 2(1-\sqrt{3})$, the emitter configuration is light-like at
$x^\mu = \frac{1}{2}\left(-3\left(\sqrt{3}-3\right), \left(\sqrt{3}+1\right), \left(\sqrt{3}+1\right), \left(\sqrt{3}+1\right)\right)$, which is the sole emission solution (with $\hat{\epsilon} = -1$). The solution with $\hat{\epsilon} = 1$ is degenerate.

(iii) For $\sigma = -\frac{3}{2}$, the emitter configuration is time-like at
$x^\mu_+ = \frac{(5\sqrt{3}+9)}{4}(5,3,3,3)$ and
$x^\mu_- = \frac{1}{524}\left(49(17\sqrt{3}-9), 3(49\sqrt{3}+159), 3(49\sqrt{3}+159), 3(49\sqrt{3}+159)\right)$, both being emission solutions (with $\hat{\epsilon} = 1$ and $\hat{\epsilon} = -1$, respectively); $x_-(x_+)$ is in the front (back) emission coordinate domain.

Table 1. RPS solution for users with $\tau^1 = -\sigma, \tau^2 = \sigma, \tau^3 = \sigma, \tau^4 = \sigma$, for different values of σ.

σ	χ^2	Δ_σ	x^0	$x^1 = x^2 = x^3$	Emission solutions
$\frac{1}{2}$	< 0	> 0	$\frac{9}{44}\left(5\sqrt{3}+3\right)$	$-\frac{1}{44}\left(9\sqrt{3}+23\right)$	$\hat{\epsilon} = -1$ One emission solution
$2(1-\sqrt{3})$	0	> 0	$-\frac{3}{2}\left(\sqrt{3}-3\right)$	$\frac{1}{2}\left(\sqrt{3}+1\right)$	$\hat{\epsilon} = -1$ One emission solution
$-\frac{3}{2}$	> 0	> 0	$\frac{5}{4}(5\sqrt{3}+9)$ $\frac{49}{524}(17\sqrt{3}-9)$	$\frac{3}{4}(5\sqrt{3}+9)$ $\frac{3}{524}(49\sqrt{3}+159)$	$\hat{\epsilon} = 1$ $\hat{\epsilon} = -1$ Two emission solutions

The main results obtained in this section can be particularized by setting $\beta = 0$ to describe the case where all four emitters are static and spatially forming a regular tetrahedron (see [9] for the static case in which the emitters are forming an orthogonal tetrahedron).

 doi:10.20944/preprints202604.0665.v1

4. RPS with One Hyperbolic and Three Static Emitters

In this example we consider that emitters 2, 3 and 4 are static. Emitter 1 is moving in hyperbolic motion with constant proper acceleration $\alpha > 0$ along the bisectrix $(1,1,1)$, in such a way that at $\tau^1 = 0$ the four emitters are spatially forming a regular tetrahedron. As $\tau^1 \to \pm\infty$, its spatial position tends to $+\infty$ along the main bisectrix.

4.1. Emitters' World-Lines and Emission/Reception Conditions

World-lines with respect to the inertial obeserver u:

$$\begin{aligned}\gamma_1 =& \frac{\gamma(\tau^1)\beta(\tau^1)}{\alpha}u + \left[\frac{\gamma(\tau^1)-1}{\sqrt{3}\alpha}+1\right](1,1,1), \quad \gamma_2 = \tau^2\, u + (1,-1,-1),\\ \gamma_3 =& \tau^3\, u + (-1,1,-1), \qquad\qquad\qquad\qquad \gamma_4 = \tau^4\, u + (-1,-1,1),\end{aligned}$$

where $\gamma(\tau^1) = \cosh(\alpha\tau^1)$ and $\beta(\tau^1) = \tanh(\alpha\tau^1)$. Expressing the coordinate time in seconds, the proper acceleration α is expressed in s^{-1}. We consider that the proper times of emitters 2, 3 and 4 are synchronised at their common origin $\tau^2 = \tau^3 = \tau^4 = 0$ and that the proper time of emitter 1 is synchronised with theirs at $\tau^1 = 0$. The distance covered by emitter 1 in one second of coordinate time $\Delta x^0 = 1\ s$, starting from zero coordinate time when it is at rest with respect to the inertial observer ($\Delta\tau^1 = \frac{\operatorname{arcsinh}(\alpha\Delta x^0)}{\alpha} = \frac{\operatorname{arcsinh}(\alpha)}{\alpha}$), is $d_1 = \frac{\cosh(\alpha\Delta\tau^1)-1}{\alpha}\ ls$. [6]

Defining

$$\Phi(\tau^1) = \frac{\gamma(\tau^1)\beta(\tau^1)}{\alpha} = \frac{\sinh(\alpha\tau^1)}{\alpha}, \quad \Sigma(\tau^1) = \frac{\gamma(\tau^1)-1}{\sqrt{3}\alpha},$$
$$q_1 = \Phi - \tau^4, \quad q_2 = \tau^2 - \tau^4, \quad q_3 = \tau^3 - \tau^4,$$

one obtains the following position vectors with respect to the fourth emitter $e_a = \gamma_a - \gamma_4$, $a = 1,2,3$:

$$e_1 = q_1\, u + (\Sigma+2, \Sigma+2, \Sigma), \quad e_2 = q_2\, u + (2,0,-2), \quad e_3 = q_3\, u + (0,2,-2), \tag{22}$$

and the following world-functions $\Omega_a = \frac{1}{2}(e_a)^2$, $a = 1,2,3$:

$$\Omega_1 = \tfrac{1}{2}\left(2(\Sigma+2)^2 + \Sigma^2 - q_1^2\right), \quad \Omega_2 = \tfrac{1}{2}(8 - q_2^2), \quad \Omega_3 = \tfrac{1}{2}(8 - q_3^2). \tag{23}$$

The emission/reception conditions $e_a^2 > 0$ and $(e_a - e_b)^2 > 0$ read:

$$\left|\Phi - \tau^4\right| < \sqrt{2(\Sigma+2)^2 + \Sigma^2}, \quad \left|\tau^2 - \tau^4\right| < \sqrt{8}, \quad \left|\tau^3 - \tau^4\right| < \sqrt{8},$$
$$\left|\Phi - \tau^2\right| < \sqrt{2(\Sigma+2)^2 + \Sigma^2}, \quad \left|\Phi - \tau^3\right| < \sqrt{2(\Sigma+2)^2 + \Sigma^2}, \quad \left|\tau^2 - \tau^3\right| < \sqrt{8}.$$

4.2. Emitters' Trajectories on the Grid $\mathcal{T}$

In this case, the equations to obtain the τ^1-coordinate of trajectories S_2, S_3 and S_4 ($(\gamma_i - \gamma_1)^2 = 0$, $i = 2,3,4$) are:

$$A\sqrt{t^2+1} + B_i\, t + C_i = 0, \quad t = \sinh(\alpha\tau^1), \tag{24}$$
$$A = \frac{6}{\alpha} - 8\sqrt{3}, \quad B_i = -6\tau^i, \quad C_i = 3\alpha(\tau^i)^2 - 24\alpha - A, \quad i = 2,3,4.$$

[6] For $\alpha = 1\ s^{-1}$, $d_1 = 0.414\ ls \approx 124.000\ km$.

 doi:10.20944/preprints202604.0665.v1

For $\alpha = \frac{\sqrt{3}}{4} \equiv \alpha_0$ ($A = 0$), the solution to (24) is

$$v_0(\tau^i) = \frac{4}{\sqrt{3}} \operatorname{arcsinh}\left(\frac{\sqrt{3}((\tau^i)^2 - 8)}{8\tau^i}\right), \quad i = 2,3,4. \tag{25}$$

Solution v_0 is valid for $\tau^i \neq 0$. It will be an emission solution iff the corresponding inertial time at the emission event, $\Phi(v_0)$, is less than the inertial time at the reception event, τ^i, $\frac{\sqrt{3}((\tau^i)^2-8)}{8\tau^i} < \tau^i$, that is, iff $\tau^i > 0$.
For $\alpha \neq \alpha_0$, the solution of (24) is

$$v_\alpha(\tau^i) = \frac{1}{\alpha} \operatorname{arcsinh}(D_i), \quad D_i = \frac{B_i\, C_i + \rho\sqrt{A^2(B_i^2 + C_i^2 - A^2)}}{A^2 - B_i^2}, \; \rho = \pm 1, \; i = 2,3,4. \tag{26}$$

The two solutions included in (26), depending on the sign ρ, originate from the solution process of the square root equation (24) and therefore have to satisfy the additional condition $\frac{B_i}{A} D_i + \frac{C_i}{A} < 0$. Additionally, solution v_α is valid for $\tau^i \neq \pm\left(\frac{1}{\alpha} - \frac{4}{\sqrt{3}}\right)$ and will be an emission solution iff $D_i < \tau^i$.

Denoting by $v(\tau)$ solution (25) or (26), depending on the value of α, and supposing the conditions for each of these solutions are satisfied, we obtain the following trajectories S_A on the grid $\mathcal{T}$:

$$\begin{aligned}
S_1(\tau) &: \left(\tau, \Phi - \sqrt{2(\Sigma+2)^2 + \Sigma^2}, \Phi - \sqrt{2(\Sigma+2)^2 + \Sigma^2}, \Phi - \sqrt{2(\Sigma+2)^2 + \Sigma^2}\right), \\
S_2(\tau) &: \left(v(\tau), \tau, \tau - \sqrt{8}, \tau - \sqrt{8}\right), \\
S_3(\tau) &: \left(v(\tau), \tau - \sqrt{8}, \tau, \tau - \sqrt{8}\right), \\
S_4(\tau) &: \left(v(\tau), \tau - \sqrt{8}, \tau - \sqrt{8}, \tau\right),
\end{aligned} \tag{27}$$

with $\Phi(\tau) = \frac{\sinh(\alpha\tau)}{\alpha}$ and $\Sigma(\tau) = \frac{\gamma(\tau)-1}{\sqrt{3}\alpha}$.

4.3. Shadow-Dodecahedron

We can write the coordinates of the 14 vertices of the shadow-dodecahedron on the grid $\mathcal{T}_1 \equiv [\tau^2] \times [\tau^3] \times [\tau^4]$, these coordinates depending on τ^1 as follows:

$$\begin{aligned}
V_1 &= (K_+, K_+, K_+), & V_2 &= (K_-, K_-, K_-), \\
V_3 &= (K_+ - \sqrt{8}, K_+, K_+), & V_4 &= (K_+, K_+ - \sqrt{8}, K_+), \\
V_5 &= (K_+, K_+, K_+ - \sqrt{8}), & V_6 &= (K_- + \sqrt{8}, K_-, K_-), \\
V_7 &= (K_-, K_- + \sqrt{8}, K_-), & V_8 &= (K_-, K_-, K_- + \sqrt{8}), \\
V_9 &= (K_+ - \sqrt{8}, K_+ - \sqrt{8}, K_+), & V_{10} &= (K_+, K_+ - \sqrt{8}, K_+ - \sqrt{8}), \\
V_{11} &= (K_+ - \sqrt{8}, K_+, K_+ - \sqrt{8}), & V_{12} &= (K_- + \sqrt{8}, K_- + \sqrt{8}, K_-), \\
V_{13} &= (K_-, K_- + \sqrt{8}, K_- + \sqrt{8}), & V_{14} &= (K_- + \sqrt{8}, K_-, K_- + \sqrt{8}),
\end{aligned}$$

with $K_\pm(\tau^1) \equiv \Phi \pm \sqrt{2(\Sigma+2)^2 + \Sigma^2}$. Of these 14 vertices, only one concides with a satellite trajectory on the grid $\mathcal{T}_1$, namely V_2 with the trajectory of satellite 1.

To describe the motion of the dodecahedron on the grid $\mathcal{T}_1$ as $\tau^1 \to \pm\infty$, note that vertices V_1 and V_2, the endpoints on the main bisectrix, satisfy $\lim_{\tau^1 \to -\infty} V_1 = l_\alpha$ and $\lim_{\tau^1 \to \infty} V_2 = -l_\alpha$, with $l_\alpha = (-\frac{1}{\alpha} + \frac{4}{\sqrt{3}})(1,1,1)$. The translational motion is therefore restricted by this limit: as $\tau^1 \to -\infty$, V_1 does not go beyond l_α and as $\tau^1 \to \infty$, V_2 does not go beyond $-l_\alpha$. Its longitudinal deformation, however, increases as $|\tau^1| \to \infty$. At $\tau^1 = 0$ the dodecahedron is smallest. Figure 4 shows the shadow-dodecahedron for $\alpha = 1$ at $\tau^1 = -2$ and $\tau^1 = 1$.

 doi:10.20944/preprints202604.0665.v1

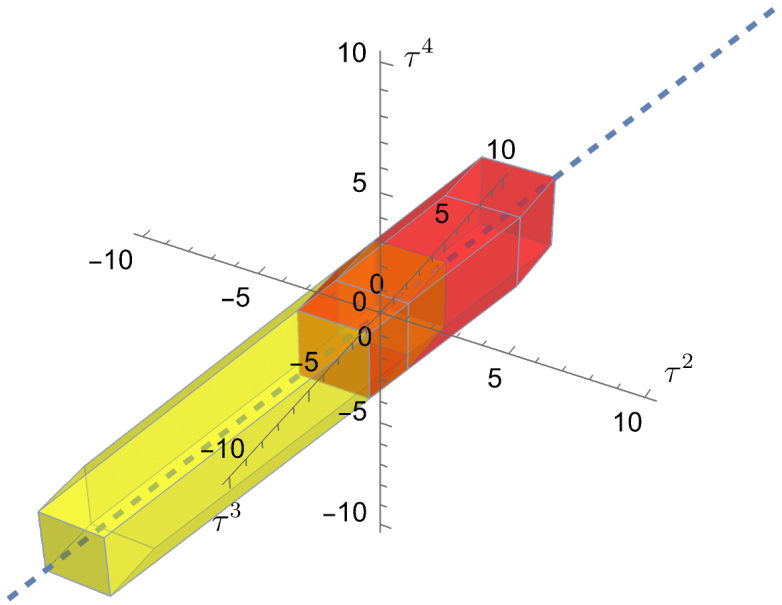

Figure 4. The shadow-dodecahedron on the grid $\mathcal{T}_1$ for $\alpha = 1$ at $\tau^1 = -2$ (yellow and orange overlap) and $\tau^1 = 1$ (red and orange overlap). The main bisectrix is also shown (dashed line).

4.4. Interpreting the RPS Solution

We can represent the characteristic regions of the RPS solution in Cartesian coordinates for this example, depending on the causal character of the configuration vector χ. Figure 5 shows these regions and the region where the jacobian determinant of the transformation from inertial to emission coordinates vanishes, $j_\Theta(x) = 0$, for $\alpha = 1$ and $x^0 = 1$. As in the previous example involving inertial motion, these regions change with every inertial instant x^0 for a given proper acceleration α. However, unlike that example, for a given x^0 the RPS solution is not defined for the whole Euclidean space. Due to the hyperbolic motion of emitter 1, there are space-time regions for which there are no (emission) solutions to the null propagation equation $(x - \gamma_1)^2 = 0$.

 doi:10.20944/preprints202604.0665.v1

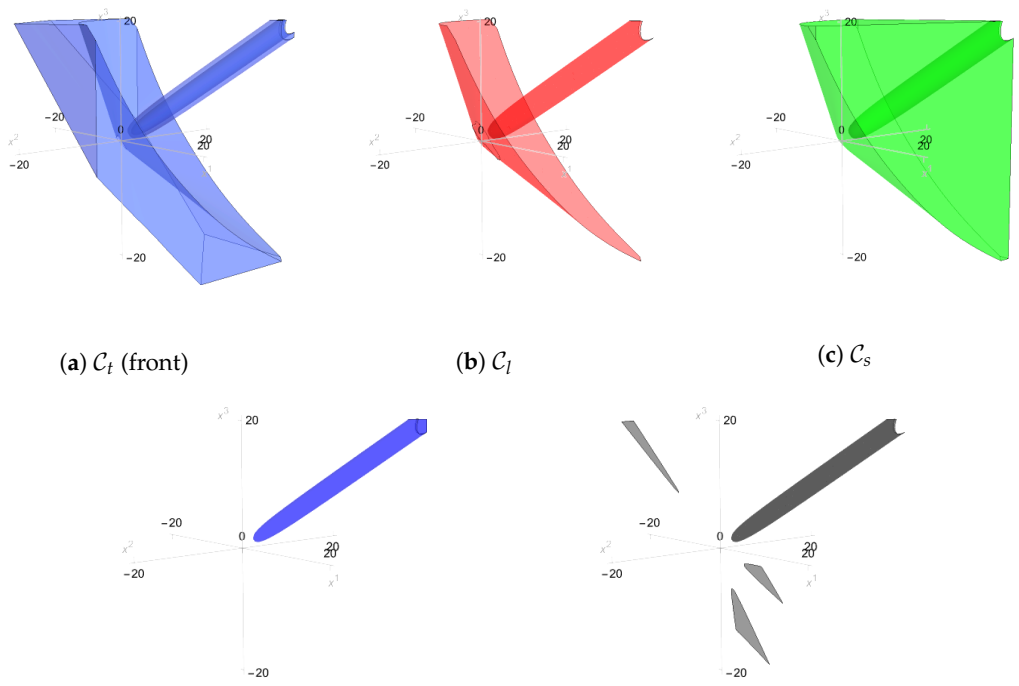

(**a**) $\mathcal{C}_t$ (front) (**b**) $\mathcal{C}_l$ (**c**) $\mathcal{C}_s$

(**d**) $\mathcal{C}_t$ (back) (**e**) $j_\Theta(x) = 0$

Figure 5. Representation of the emission configuration regions, at $x^0 = 1$, for a RPS with one inertial emitter moving in hyperbolic motion with proper acceleration $\alpha = 1$ along the bisectrix $(1, 1, 1)$ and three static emitters. The emission configuration regions $\mathcal{C}_s$ (space-like), $\mathcal{C}_l$ (light-like) and $\mathcal{C}_t$ (time-like) are colored in green, red and blue, respectively. The 3-surface where $j_\Theta(x)$ vanishes is shown in black.

Figure 6 includes a two dimensional slice of the emission configuration regions shown in Figure 5, through the plane containing emitters 1, 2 and 3 at $x^0 = 1$ ($\alpha = 1$). Black points represent satellite trajectories. The intersection with $j_\Theta(x) = 0$ is also represented.

 doi:10.20944/preprints202604.0665.v1

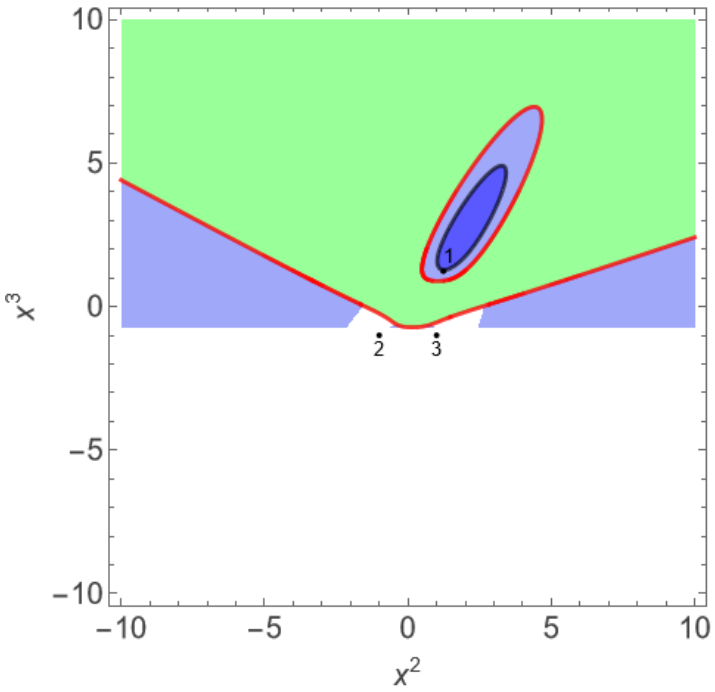

Figure 6. Slice of the emission configuration regions (shown in Figure 5) through the plane containing emitters 1, 2 and 3 at $x^0 = 1$ ($\alpha = 1$). Black points represent the satellites as indicated. In the white region the RPS solution is not defined.

And to remark the essential properties of the RPS solution in this hyperbolic case, we consider the inertial coordinate location of those users whose emission coordinates satisfy the restrictions $\Phi(\tau^1) = -\sigma$, $\tau^2 = \tau^3 = \tau^4 = \sigma$, for which

$$\chi_\mu = -8\left(2 + \frac{\sqrt{3}}{2\alpha}(\sqrt{\alpha^2\sigma^2+1} - 1), \sigma, \sigma, \sigma\right), \tag{28}$$

where we have used (22) and (1). To calculate the particular solution y_*, we first compute H using (22), (23), (8) and (7). Then, choosing the transversal vector $\xi = u$, Equation (6) yields:

$$y_{*_\mu} = \frac{2}{\alpha^2 D}(0, y_{*_1}, y_{*_2}, y_{*_3}), \quad D = -4\left(4 + \frac{\sqrt{3}}{\alpha}(\sqrt{\alpha^2\sigma^2+1} - 1)\right), \tag{29}$$

$$\begin{aligned} y_{*_1} &= y_{*_2} = 3\alpha^2\sigma^2 - (4\sqrt{3}\alpha - 2)\sqrt{\alpha^2\sigma^2+1} - 8\alpha^2 + 4\sqrt{3}\alpha - 2, \\ y_{*_3} &= 3\alpha^2\sigma^2 + 2\sqrt{\alpha^2\sigma^2+1} + 8\alpha^2 - 2. \end{aligned} \tag{30}$$

With this choice of ξ, the transversality condition imposes no restriction on this solution ($D \neq 0$ for any $\{\alpha, \sigma\}$). Taking into account (9) the solution reads:

$$x^\mu(-\sigma, \sigma, \sigma, \sigma) = (\sigma, -1, -1, 1) + y_* - \frac{\lambda_1}{\lambda_2}\chi, \tag{31}$$

$$\begin{aligned} \lambda_1 &= 27\alpha^4\sigma^4 + 4\alpha^2\sigma^2(-6 + 12\alpha^2 + 9\sqrt{\alpha^2\sigma^2+1} + 4\sqrt{3}\alpha(1 - 3\sqrt{\alpha^2\sigma^2+1})) \\ &\quad + 8(-3 + 8\sqrt{3}\alpha - 28\alpha^2 + 16\sqrt{3}\alpha^3)\sqrt{\alpha^2\sigma^2+1} + 8(3 - 8\sqrt{3}\alpha + 28\alpha^2 - 16\sqrt{3}\alpha^3 + 24\alpha^4), \\ \lambda_2 &= -2\alpha^2 D\left(18\alpha^2\sigma^3 - 4\sigma[3(1 - \sqrt{\alpha^2\sigma^2+1}) + 4\alpha(\alpha + \sqrt{3}(\sqrt{\alpha^2\sigma^2+1} - 1))] - \hat{\epsilon}\alpha^2 D\sqrt{\Delta_\sigma}\right), \\ \Delta_\sigma &= \frac{\lambda_1}{16\alpha^4} - 8\sigma^2. \end{aligned}$$

 doi:10.20944/preprints202604.0665.v1

In this case, the emission-reception conditions are reduced to:

$$|\sigma| < \frac{1}{2}\sqrt{\sigma^2 + \frac{2}{3\alpha^2}(4\sqrt{3}\alpha - 3)(\sqrt{\alpha^2\sigma^2+1} - 1) + 8}\,. \tag{32}$$

Table 2 shows the result setting $\alpha = 1$ for different values of σ. In this particular case, the previous emission-reception condition imposes
$|\sigma| < \frac{2}{3}\sqrt{\frac{1}{3}(-10\sqrt{3} + \sqrt{838 - 424\sqrt{3}} + 32)} \approx 1.92$.

(i) For $\tau = \frac{3}{4}$, the emitter configuration is space-like at $x^\mu = \frac{1}{1448}\Big(1648\sqrt{3}+821, -5(103\sqrt{3}+40), -5(103\sqrt{3}+40), -5(103\sqrt{3}+40)\Big)$, which is the sole emission solution (with $\hat{\epsilon} = -1$). The solution with $\hat{\epsilon} = 1$ is a reception solution.

(ii) For $\tau = \frac{2}{9}\Big(-4\sqrt{3} - \sqrt{21 - 6\sqrt{3}} + 3\Big) \approx -1.60$, the emitter configuration is light-like at $x^\mu \approx (1.81, 1.39, 1.39, 1.39)$, which is the sole emission solution (with $\hat{\epsilon} = -1$). The solution with $\hat{\epsilon} = 1$ is degenerate.

(iii) For $\tau = -\frac{17}{10}$, the emitter configuration is time-like at $x^\mu_+ \approx (9.63, 6.14, 6.14, 6.14)$ and $x^\mu_- \approx (1.84, 1.48, 1.48, 1.48)$, both being emission solutions (with $\hat{\epsilon} = 1$ and $\hat{\epsilon} = -1$, respectively); $x_-(x_+)$ is in the front (back) emission coordinate domain.

Table 2. RPS solution with $\alpha = 1$ for users with $\sinh(\tau^1) = -\sigma, \tau^2 = \sigma, \tau^3 = \sigma, \tau^4 = \sigma$.

σ	χ^2	Δ_σ	x^0	$x^1 = x^2 = x^3$	Emission solutions
$\frac{3}{4}$	< 0	> 0	$\frac{1}{1448}\Big(1648\sqrt{3}+821\Big)$	$-\frac{5}{1448}\Big(103\sqrt{3}+40\Big)$	$\hat{\epsilon} = -1$ One emission solution
≈ -1.60	0	> 0	≈ 1.81	≈ 1.39	$\hat{\epsilon} = -1$ One emission solution
$-\frac{17}{10}$	> 0	> 0	≈ 9.63 ≈ 1.84	≈ 6.14 ≈ 1.48	$\hat{\epsilon} = 1$ $\hat{\epsilon} = -1$ Two emission solutions

5. RPS with One Static and Three Rotating Emitters

In this example we consider the spatial configuration of emitters 1, 2 and 3 following uniform circular motion on the $\{x, y\}$-plane, at constant radial distance r_0 and equally spaced at an angle $\frac{2\pi}{3}$, and emitter 4 static at distance d on the z-axis.

5.1. Emitters' World-Lines and Emission/Reception Conditions

If ω is the constant angular velocity with respect to the inertial observer u, we can write the world-lines as follows:

$$\begin{aligned}
\gamma_1 =& \gamma\tau^1\, u + r_0\Big(\cos\Big(\omega\gamma\tau^1\Big), \sin\Big(\omega\gamma\tau^1\Big), 0\Big),\\
\gamma_2 =& \gamma\tau^2\, u + r_0\Big(\cos\Big(\omega\gamma\tau^2 - \frac{2\pi}{3}\Big), \sin\Big(\omega\gamma\tau^2 - \frac{2\pi}{3}\Big), 0\Big),\\
\gamma_3 =& \gamma\tau^3\, u + r_0\Big(\cos\Big(\omega\gamma\tau^3 - \frac{4\pi}{3}\Big), \sin\Big(\omega\gamma\tau^3 - \frac{4\pi}{3}\Big), 0\Big), \quad \gamma_4 = \tau^4\, u + (0, 0, d),
\end{aligned} \tag{33}$$

where $\gamma = (1 - \beta^2)^{-\frac{1}{2}}$ and $\beta = \omega r_0$ ($\omega r_0 < 1$). The velocity β is expressed as a fraction of the speed of light in vacuum c ($\beta < 1$). We consider that the proper times of emitters 1, 2 and 3 are synchronised at their common origin $\tau^1 = \tau^2 = \tau^3 = 0$ and are synchronised with emitter 4 at $\tau^4 = 0$. Expressing the coordinate time in seconds and the spatial coordinates in kilometres, the number of revolutions

 doi:10.20944/preprints202604.0665.v1

s_1 completed by emitter 1 in one second of coordinate time $\Delta x^0 = 1\ s$ ($\Delta\tau^1 = \gamma^{-1}\Delta x^0 = \gamma^{-1}\ s$) is $s_1 \approx \frac{\beta}{2\pi r_0} 3 \cdot 10^5$, truncated to an integer. [7]

Defining

$$q_1 = \Gamma_1 - \tau^4, \quad q_2 = \Gamma_2 - \tau^4, \quad \Gamma_3 - \tau^4, \quad \Gamma_a = \gamma\tau^a, \quad a = 1,2,3,$$

one obtains the following position vectors with respect to the fourth emitter, $e_a = \gamma_a - \gamma_4$, $a = 1,2,3$:

$$\begin{aligned} e_1 =& q_1\, u + r_0\left(\cos(\omega\Gamma_1), \sin(\omega\Gamma_1), -\frac{d}{r_0}\right), \\ e_2 =& q_2\, u + r_0\left(\cos\left(\omega\Gamma_2 - \frac{2\pi}{3}\right), \sin\left(\omega\Gamma_2 - \frac{2\pi}{3}\right), -\frac{d}{r_0}\right), \\ e_3 =& q_3\, u + r_0\left(\cos\left(\omega\Gamma_3 - \frac{4\pi}{3}\right), \sin\left(\omega\Gamma_3 - \frac{4\pi}{3}\right), -\frac{d}{r_0}\right), \end{aligned} \tag{34}$$

and the world-functions

$$\Omega_a = \tfrac{1}{2}(r_0^2 + d^2 - q_a^2), \quad a = 1,2,3. \tag{35}$$

In this example, the emission/reception conditions (3) impose:

$$\begin{aligned} |\Gamma_a - \tau^4| <& \sqrt{r_0^2 + d^2}, \quad a = 1,2,3, \\ |\Gamma_1 - \Gamma_2| <& \sqrt{2} r_0 \sqrt{1 + \sin\left(\omega(\Gamma_1 - \Gamma_2) + \frac{\pi}{6}\right)}, \\ |\Gamma_1 - \Gamma_3| <& \sqrt{2} r_0 \sqrt{1 + \sin\left(\omega(\Gamma_3 - \Gamma_1) + \frac{\pi}{6}\right)}, \\ |\Gamma_2 - \Gamma_3| <& \sqrt{2} r_0 \sqrt{1 + \sin\left(\omega(\Gamma_2 - \Gamma_3) + \frac{\pi}{6}\right)}. \end{aligned}$$

5.2. Emitters' Trajectories on the Grid $\mathcal{T}$

The emission coordinate τ^b of the a-emitter ($a, b = 1,2,3,4$) satisfies the equation $(\gamma_a(\tau^a) - \gamma_b(\tau^b))^2 = 0$. Due to the transcendental functions appearing in the world-lines of emitters 1, 2 and 3 (33), the τ^1, τ^2 and τ^3-coordinates of the trajectories of emitters 1, 2 and 3 on the grid $\mathcal{T}$ (S_1, S_2 and S_3) can only be computed numerically, by solving the following equations:

$$(\Gamma_1 - \Gamma_2)^2 = 2r_0^2\left(1 + \sin\left(\omega(\Gamma_1 - \Gamma_2) + \frac{\pi}{6}\right)\right), \tag{36}$$

$$(\Gamma_3 - \Gamma_1)^2 = 2r_0^2\left(1 + \sin\left(\omega(\Gamma_3 - \Gamma_1) + \frac{\pi}{6}\right)\right), \tag{37}$$

$$(\Gamma_2 - \Gamma_3)^2 = 2r_0^2\left(1 + \sin\left(\omega(\Gamma_2 - \Gamma_3) + \frac{\pi}{6}\right)\right). \tag{38}$$

Note that Equations (36)-(38) implicitly describe a lineal relationship between τ^a and τ^b, $a, b = 1,2,3$. Specifically, the solution of one coordinate in terms of the other is a straight line of unit slope, whose intercept has to be computed numerically. So, the solution for τ^2 of Equation (36) is $\tau^2(\tau^1) = \tau^1 + m$, with m the numerical solution[8] to:

$$m^2 = \frac{2r_0^2}{\gamma^2}\left(1 + \sin\left(-\omega\gamma m + \frac{\pi}{6}\right)\right). \tag{39}$$

[7] For $r_0 = 10,000\ km$ and $\beta = \frac{1}{2}$, $s_1 = 2$.

[8] Of the two solutions for m (one positive and one negative), we choose the negative one so that τ^2 lies on the past null cone of S_1.

 doi:10.20944/preprints202604.0665.v1

For $r_0 = d = 1$ and $\omega = \frac{1}{2}$ ($\gamma = \frac{2}{\sqrt{3}}$), $m \approx -1.732$.[9]
It is clear that the solution for τ^1 of Equation (37) is $\tau^1(\tau^3) = \tau^1 + m$ and the solution for τ^3 of (38) is $\tau^3(\tau^2) = \tau^2 + m$. Analogously, the solution for τ^1 of (36) is $\tau^1(\tau^2) = \tau^2 + n$, with n the (negative) numerical solution to:

$$n^2 = \frac{2r_0^2}{\gamma^2}\left(1 + \sin\left(\omega\gamma n + \frac{\pi}{6}\right)\right). \tag{40}$$

For $r_0 = d = 1$ and $\omega = \frac{1}{2}$ ($\gamma = \frac{2}{\sqrt{3}}$), $n \approx -1.140$.
Then, the solution for τ^3 of Equation (37) is $\tau^3(\tau^1) = \tau^1 + n$ and the solution for τ^2 of (38) is $\tau^2(\tau^3) = \tau^2 + n$. The following trajectories S_A on the grid $\mathcal{T}$ are thus obtained:

$$\begin{aligned}
S_1(\tau) &: \left(\tau, \tau + m, \tau + n, \gamma\tau - \sqrt{d^2 + r_0^2}\right),\\
S_2(\tau) &: \left(\tau + n, \tau, \tau + m, \gamma\tau - \sqrt{d^2 + r_0^2}\right),\\
S_3(\tau) &: \left(\tau + m, \tau + n, \tau, \gamma\tau - \sqrt{d^2 + r_0^2}\right),\\
S_4(\tau) &: \left(\gamma^{-1}\left(\tau - \sqrt{d^2 + r_0^2}\right), \gamma^{-1}\left(\tau - \sqrt{d^2 + r_0^2}\right), \gamma^{-1}\left(\tau - \sqrt{d^2 + r_0^2}\right), \tau\right),
\end{aligned} \tag{41}$$

where m and n are obtained numerically from (39) and (40) for given values of the parametres r_0 and ω.

5.3. Shadow-Dodecahedron

Next, we analyse the shadow-dodecahedron on the grid $\mathcal{T}_4 \equiv [\tau^1] \times [\tau^2] \times [\tau^3]$ for a given τ^4. Again, due to the trascendental functions appearing in the emission/reception conditions, the vertices of the dodecahedron have to be computed numerically. The resulting dodecahedron is composed of 3 hexagons, 3 rhomboids and 6 pentagons, leading to the following 20 vertices:

$$\begin{aligned}
V_1 &= (L_+, L_+, L_+), & V_2 &= (L_-, L_-, L_-),\\
V_3 &= (L_+ + n, L_+, L_+), & V_4 &= (L_+, L_+ + n, L_+),\\
V_5 &= (L_+, L_+, L_+ + n), & V_6 &= (L_- - n, L_-, L_-),\\
V_7 &= (L_-, L_- - n, L_-), & V_8 &= (L_-, L_-, L_- - n),\\
V_9 &= (L_+ + n, L_+, L_+ + m), & V_{10} &= (L_+ + m, L_+ + n, L_+),\\
V_{11} &= (L_+, L_+ + m, L_+ + n), & V_{12} &= (L_- - n, L_- - m, L_-),\\
V_{13} &= (L_-, L_- - n, L_- - m), & V_{14} &= (L_- - m, L_-, L_- - n),\\
V_{15} &= (L_+ + n + (n - m), L_+, L_+ + m), & V_{16} &= (L_+ + m, L_+ + n + (n - m), L_+),\\
V_{17} &= (L_+, L_+ + m, L_+ + n + (n - m)), & V_{18} &= (L_- - n - (n - m), L_- - m, L_-),\\
V_{19} &= (L_-, L_- - n - (n - m), L_- - m), & V_{20} &= (L_- - m, L_-, L_- - n - (n - m)),
\end{aligned}$$

with $L_\pm(\tau^4) \equiv \gamma^{-1}(\tau^4 \pm \sqrt{r_0^2 + d^2})$ and m and n given by (39) and (40). The coordinates of the vertices V_a, $a = 3, 4, ..., 20$, are obtained by adding or substracting the distances m and n and their difference to the coordinates of the end vertices V_1 and V_2 on the main bisectrix. In the shadow-dodecahedrons of the previous examples, with fourteen vertices forming six squares and six rhomboids, only one distance[10] is added or substracted to the coordinates of the end vertices V_1 and V_2, hence we can say that in previous examples m and n coincide. Note that, unlike in previous examples, in this case of three rotating and one inertial emitter, the shadow-dodecahedron is described on the $\mathcal{T}_4$-grid, where

[9] Note that if r_0 is expressed in light-seconds, m is expressed in seconds.
[10] This distance is $\sqrt{8}$.

 doi:10.20944/preprints202604.0665.v1

the $\tau-$coordinate not forming part of the grid[11] is the coordinate of the static and not of the moving emitter.

For different values of τ^4, the shadow-dodecahedron moves along the main bisectrix of the $\mathcal{T}_4$-grid without changing its shape (the relative positions of its vertices remain constant for every τ^4). Figure 7 shows the shadow-dodecahedron for $r_0 = d = 1$ and $\omega = \frac{1}{2}$ ($\gamma = \frac{2}{\sqrt{3}}$) at $\tau^4 = -2$, $\tau^4 = 2$ and $\tau^4 = 6$:

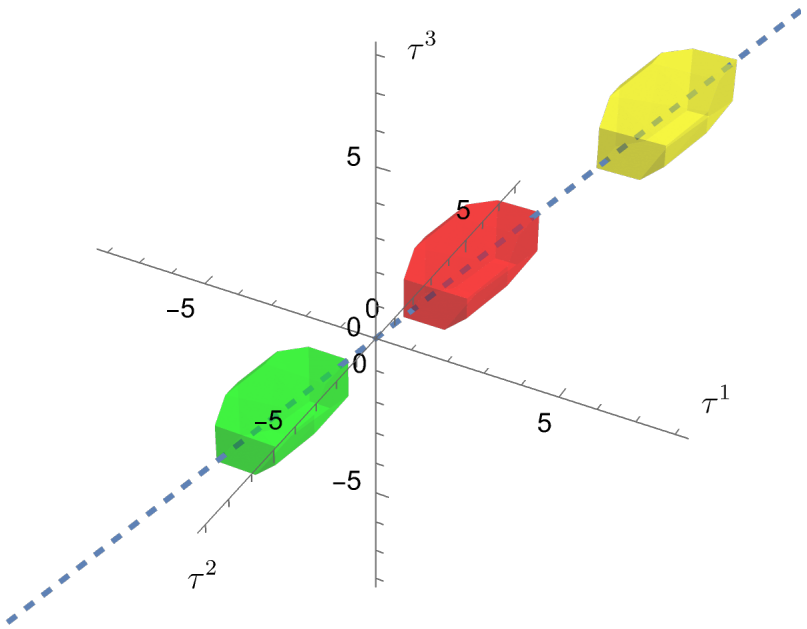

Figure 7. The shadow-dodecahedron on the grid $\mathcal{T}_4$ for $r_0 = d = 1$ and $\omega = \frac{1}{2}$ at $\tau^4 = -2$ (green), $\tau^4 = 2$ (red) and $\tau^4 = 6$ (yellow). The main bisectrix is also shown (dashed line).

5.4. Interpreting the RPS Solution

In this example, representing the characteristic regions of the RPS solution in Cartesian coordinates for a given inertial time is not straightforward. Since the null propagation equations (2) can not be solved analitically for τ^A (the characteristic emission function Θ, $\tau^A = \Theta^A(x)$, can not be obtained), we can not directly express the configuration vector χ in Cartesian coordinates for a given coordinate time x^0. Instead, we proceed numerically, first classifying a sufficient number of quads of emission coordinates $\{\tau^1, \tau^2, \tau^3, \tau^4\}$ according to the configuration vector's causal character associated to each of them. Then, we transform each of these quads to inertial coordinates using (5) and label the space-time points thus obtained with the same color scheme as in previous examples. For each characteristic region we compute a large number of points and select those with a given (common) inertial time x^0. This process unavoidably leads to approximations, for which reason the following representations have to be considered qualitatively.[12] Figure 8 illustrates these regions for $x^0 = 5$ ($r_0 = d = 1$ and $\omega = \frac{1}{2}$ ($\gamma = \frac{2}{\sqrt{3}}$)).

[11] It is considered a parameter.
[12] A detailed numerical study is beyond the scope of this work.

 doi:10.20944/preprints202604.0665.v1

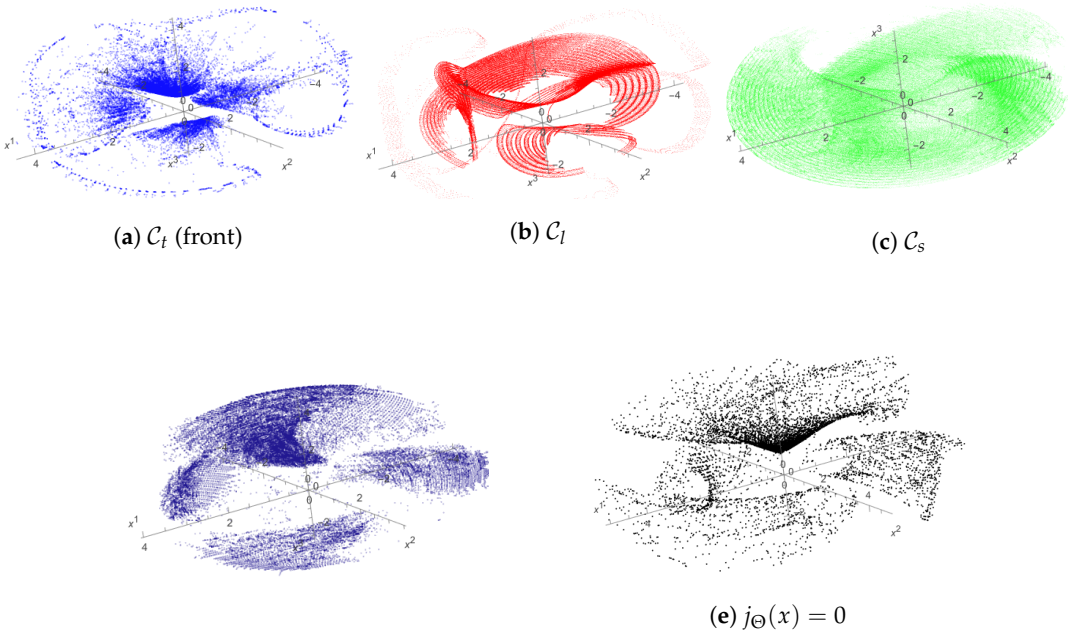

(**a**) $\mathcal{C}_t$ (front) (**b**) $\mathcal{C}_l$ (**c**) $\mathcal{C}_s$

(**d**) $\mathcal{C}_t$ (back) (**e**) $j_\Theta(x) = 0$

Figure 8. Illustration of the emission configuration regions, at $x^0 = 5$, of a RPS with three uniformly rotating emitters and one static emitter, for $r_0 = d = 1$ and $\omega = \frac{1}{2}$ ($\gamma = \frac{2}{\sqrt{3}}$). The emission configuration regions $\mathcal{C}_s$ (space-like), $\mathcal{C}_l$ (light-like) and $\mathcal{C}_t$ (time-like) are colored in green, red and blue, respectively. The 3-surface where $j_\Theta(x)$ vanishes is shown in black.

Figure 9 includes two two-dimensional slices of the emission configuration regions illustrated in Figure 8, one through the plane $x^3 = 0$ containing emitters 1, 2 and 3 and the other through the plane $x^3 = 2$, both at $x^0 = 5$ with $r_0 = d = 1$ and $\omega = \frac{1}{2}$ ($\gamma = \frac{2}{\sqrt{3}}$).

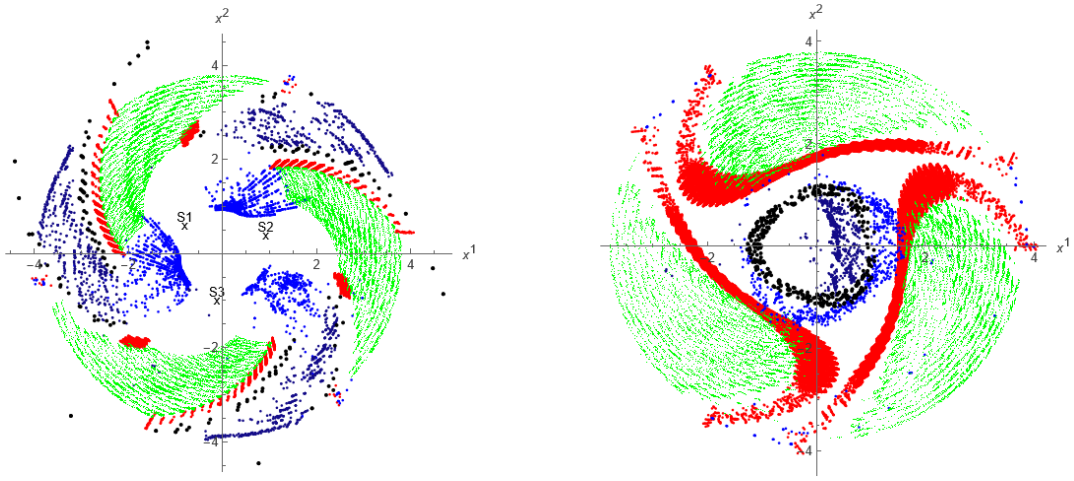

Figure 9. Slices of the emission configuration regions shown in Figure 8 at $x^0 = 5$ with $r_0 = d = 1$ and $\omega = \frac{1}{2}$ ($\gamma = \frac{2}{\sqrt{3}}$). Left: slice through the plane $x^3 = 0$ containing emitters 1, 2 and 3 . Crosses indicate approximate satellite positions. Right: slice through the plane $x^3 = 2$.

 doi:10.20944/preprints202604.0665.v1

And to remark the essential properties of the RPS solution in this example, we consider the inertial coordinate location of those users whose emission coordinates satisfy the restrictions $\tau^1 = \sigma, \tau^2 = -\sigma, \tau^3 = -\sigma$ and $\tau^4 = \gamma\sigma \equiv \Gamma_4(\sigma)$. Using (34) and (1) we calculate the configuration vector:

$$\chi_\mu = \sqrt{3} r_0 (\chi_0, \chi_1, \chi_2, \chi_3), \tag{42}$$

$$\begin{aligned} \chi_0 &= -\frac{dr_0}{2}(1 + 2\cos(2\omega\Gamma_4)), \qquad \chi_1 = 2d\ \Gamma_4 \cos(\omega\Gamma_4), \\ \chi_2 &= -2d\ \Gamma_4 \sin(\omega\Gamma_4), \qquad \chi_3 = 2r_0\Gamma_4 \cos(2\omega\Gamma_4). \end{aligned} \tag{43}$$

To calculate the particular solution y_*, the configuration bivector H is first computed using (34), (35), (8) and (7). Choosing the transversal vector $\xi = u$, Equation (6) yields:

$$y_{*\mu} = \frac{\sqrt{3} r_0}{D}(0, y_{*_1}, y_{*_2}, y_{*_3}), \quad D = -\frac{\sqrt{3}}{2} d r_0^2 \Big(1 + 2\cos(2\omega\Gamma_4)\Big), \tag{44}$$

$$\begin{aligned} y_{*_1} &= -2d\ \Gamma_4^2 \cos(\omega\Gamma_4), \quad y_{*_2} = 2d\ \Gamma_4^2 \sin(\omega\Gamma_4), \\ y_{*_3} &= \frac{r_0}{4}\Big(d^2 + r_0^2 + 2(d^2 + r_0^2 - 4\Gamma_4^2)\cos(2\omega\Gamma_4)\Big). \end{aligned} \tag{45}$$

With this choice of ξ, the transversality condition restricts this solution to

$$\{\sigma \in \mathbb{R} | \sigma \neq \sigma_t \equiv \pm\frac{\pi}{\gamma\omega}(\frac{1}{3} + n), n \in \mathbb{Z}^+\}.$$

At $\sigma = \sigma_t$ emitters 1 and 3 are at the same spatial location $(-\frac{1}{2}, \frac{\sqrt{3}}{2}, 0)$, leading to a degenerate situation. The solution (5) reads:

$$x^\alpha(\sigma, -\sigma, -\sigma, \gamma\sigma) = (\gamma\sigma, 0, 0, d) + y_* - \frac{\lambda_1}{\lambda_2}\chi, \tag{46}$$

$$\begin{aligned} \lambda_1 &= \frac{3}{16} r_0^2 \Big(64 d^2 \Gamma_4^4 + r_0^2 \Big(2\Big(d^2 - 4\Gamma_4^2 + r_0^2\Big)\cos(2\omega\Gamma_4) + d^2 + r_0^2\Big)^2\Big), \\ \lambda_2 &= D\Big(\frac{3}{2} r_0^4 \Gamma_4 \cos(2\omega\Gamma_4)\Big(2\Big(d^2 - 4\Gamma_4^2 + r_0^2\Big)\cos(2\omega\Gamma_4) + d^2 + r_0^2\Big) - 12 d^2 r_0 \Gamma_4^3 + \hat{\epsilon} D\sqrt{\Delta_\sigma}\Big), \\ \Delta_\sigma &= \lambda_1 - 3 r_0^2 \Gamma_4^2 (d^2 + r_0^2). \end{aligned}$$

In this case, the emission-reception conditions (3) are as follows:

$$|\Gamma_4| < \frac{1}{2} r_0 \sqrt{2(1 + \sin\Big(\pm 2\omega\Gamma_4 + \frac{\pi}{6}\Big)}, \quad |\Gamma_4| < \frac{1}{2}\sqrt{r_0^2 + d^2}. \tag{47}$$

Table 3 shows the result setting $r_0 = d = 1$ and $\omega = \frac{1}{2}$ ($\gamma = \frac{2}{\sqrt{3}}$) for different values of σ. In this particular case, the previous emission-reception conditions impose $-\sigma_c < \sigma < \sigma_c$, with $\sigma_c \approx 0.570$. However, unlike in previous examples, the "physical" requirement $\Delta_\sigma \geq 0$ further restricts the domain to $-\sigma_p \leq \sigma \leq \sigma_p$, with $\sigma_p \approx 0.453$, in this case.

(i) For $\sigma = -\frac{2}{5}$, the emitter configuration is space-like at $x^\alpha \approx (2.654, -1.710, -0.402, -1.573)$, which is the sole emission solution (with $\hat{\epsilon} = -1$). The solution with $\hat{\epsilon} = 1$ is a reception solution.

(ii) For $\sigma \approx 0.447$, the emitter configuration is light-like at $x^\alpha \approx (3.764, 2.746, -0.726, 2.470)$, which is the sole emission solution (with $\hat{\epsilon} = -1$). The solution with $\hat{\epsilon} = 1$ is degenerate.

(iii) For $\sigma \approx 0.450$, the emitter configuration is time-like at $x_+^\alpha \approx (20.506, 15.055, -4.002, 13.522)$ and $x_-^\alpha \approx (2.992, 2.197, -0.584, 1.973)$, both being emission solutions (with $\hat{\epsilon} = 1$ and $\hat{\epsilon} = -1$, respectively); x_- (x_+) is in the front (back) emission coordinate domain.

 doi:10.20944/preprints202604.0665.v1

Table 3. RPS solution with $r_0 = d = 1$ and $\omega = \frac{1}{2}$ ($\gamma = \frac{2}{\sqrt{3}}$) for users with $\tau^1 = \sigma, \tau^2 = -\sigma, \tau^3 = -\sigma$ and $\tau^4 = \gamma\sigma$.

σ	χ^2	Δ_σ	x^0	(x^1, x^2, x^3)	**Emission solutions**
$-\frac{2}{5}$	< 0	> 0	≈ 2.654	$\approx (-1.710, -0.402, -1.573)$	$\hat{\epsilon} = -1$ One emission solution
≈ 0.447	0	> 0	≈ 3.764	$\approx (2.746, -0.726, 2.470)$	$\hat{\epsilon} = -1$ One emission solution
≈ 0.450	> 0	> 0	≈ 20.506	$\approx (15.055, -4.002, 13.522)$	$\hat{\epsilon} = 1$
			≈ 2.992	$\approx (2.197, -0.584, 1.973)$	$\hat{\epsilon} = -1$ Two emission solutions

6. Summary and Conclusions

A basic construction of a RPS involving four static emitters in flat space-time was presented in [9]. The same procedure has been extended in the present work by including inertial, accelerated and rotating emitters. All these constructions provide clarifying examples of the notions involved in RPS theory (null propagation equations, bifurcation of solutions, grid space of emission coordinates, emission/reception conditions, shadows reciprocally cast by pairs of emitters, shadow-dodecahedron, emission coordinate region, central, front, and back regions, orientation, etc.). The examples analyzed offer a method to explore more involved constructions in flat and curved space-times. Despite the inherent differences with more complicated constructions, these elemental examples play a crucial role in RPS theory, similar to the one played in plant biology by the model organism *Arabidopsis thaliana*. Just as the model plant is essential to the molecular-biological study of more complex traits, the RPS constructions considered here contain valuable information for developing RPSs in a (known or unknown) gravitational field geometry. Furthermore, our incipient constructions of the emission coordinate regions attached to a specific RPS can be complemented with additional theoretical information, such as as the IDEAL (Intrinsic, Deductive, Explicit, ALgoritmic) characterization of gravitational fields developed in [22–25], which is necessary in order to make gravimetry (determine the true gravitational potentials) in a unknown space-time region (see [6] for details concerning this idea).

Author Contributions: Both authors contributed equally to develop the idea of the manuscript and have read and agreed to the published version of the manuscript.

Funding: We would like to thank the support from the Conselleria d'Educació, Universitats i Ocupació of the Generalitat Valenciana through project CIAICO/2022/252 and the Research Vice-Rectorate grant program (PAID-11-25) of the Polytechnic University of Valencia.

Institutional Review Board Statement: Not applicable

Informed Consent Statement: Not applicable

Data Availability Statement: Not applicable

Acknowledgments: We would like to thank the /Universe/ Editorial Office at MDPI for the invitation to submit this manuscript free of charge.

Conflicts of Interest: The authors declare no conflict of interest.

Appendix A. Notation

The main sign conventions and notation adopted in this paper are:

(i) g is the Minkowski space-time metric, with signature $(-,+,+,+)$. We use units in which the speed of light in vacuum is $c = 1$.

 doi:10.20944/preprints202604.0665.v1

(ii) η is the metric volume element of g, defined by $\eta_{\alpha\beta\gamma\delta} = -\sqrt{-\det g}\,\epsilon_{\alpha\beta\gamma\delta}$, where $\epsilon_{\alpha\beta\gamma\delta}$ stands for the Levi-Civita permutation symbol, $\epsilon_{0123} = 1$. The Hodge dual operator associated to η is denoted by an asterisk $*$. For instance, in index notation (where summing over repeated indices is understood), if x, y, z are space-time vectors, one has

$$[*(x \wedge y \wedge z)]_\alpha = \eta_{\alpha\beta\gamma\delta} x^\beta y^\gamma z^\delta, \tag{A1}$$

where $\wedge$ stands for the *wedge or exterior product* (defined by the antisymmetrized tensor product of antisymmetric tensors).

(iii) $i()$ denotes the interior or contracted product, that is, if x is a vector and T a covariant 2-tensor, one has $[i(x)T]_\nu = x^\mu T_{\mu\nu}$ (contracting the first left tensor index). If k is another space-time vector, then we have the following properties

$$i(k) * (x \wedge y) = - *(k \wedge x \wedge y), \tag{A2}$$

$$i(k) * (x \wedge y \wedge z) = * (k \wedge x \wedge y \wedge z). \tag{A3}$$

(iv) In index notation, the interior or contracted (or scalar) product of a contravariant vector (x^α) and a covariant vector (y_β) is the contraction $i(x)y = x \cdot y = x^\alpha y_\alpha$. A contravariant vector (x^α) is converted into a covariant vector (x_α) with the metric: $x_\alpha = g_{\alpha\beta} x^\beta$.

References

1. Coll, B.; Pozo, J.M. Relativistic positioning systems: the emission coordinates. *Classical and Quantum Gravity* **2006**, *23*, 7395. https://doi.org/10.1088/0264-9381/23/24/012.
2. Coll, B.; Ferrando, J.J.; Morales-Lladosa, J.A. Newtonian and relativistic emission coordinates. *Phys. Rev. D* **2009**, *80*, 064038. https://doi.org/10.1103/PhysRevD.80.064038.
3. Synge, J. *Relativity: The General Theory*; North-Holland, Amsterdam, The Netherlands, 1960.
4. Bahder, T.B. Navigation in curved space-time. *American Journal of Physics* **2001**, *69*, 315–321. https://doi.org/10.1119/1.1326078.
5. Blumenthal, L.M. *Theory and Applications of Distance Geometry*, second ed.; Chelsea Publishing Company: New York, 1970.
6. Coll, B. *Epistemic Relativity: An Experimental Approach to Physics*; Springer International Publishing, 2019; pp. 291–315. https://doi.org/10.1007/978-3-030-11500-5_8.
7. Coll, B. *Elements for a theory of relativistic coordinate systems: formal and physical aspects*; World Scientific, 2001; pp. 53–65. https://doi.org/10.1142/9789812810021_0005.
8. Coll, B. Relativistic positioning systems: perspectives and prospects. *Acta Futura* **2013**, *7*, 35–47. https://doi.org/10.2420/AF07.2013.35.
9. Serrano Montesinos, R.; Morales-Lladosa, J.A. Minkowskian Approach to the Pseudorange Navigation Equations. *Universe* **2024**, *10*. https://doi.org/10.3390/universe10040179.
10. Coll, B.; Ferrando, J.J.; Morales-Lladosa, J.A. Positioning systems in Minkowski spacetime: from emission to inertial coordinates. *Classical and Quantum Gravity* **2010**, *27*, 065013. https://doi.org/10.1088/0264-9381/27/6/065013.
11. Coll, B.; Ferrando, J.J.; Morales-Lladosa, J.A. Positioning systems in Minkowski space-time: Bifurcation problem and observational data. *Phys. Rev. D* **2012**, *86*, 084036. https://doi.org/10.1103/PhysRevD.86.084036.
12. Serrano Montesinos, R.; Ferrando, J.J.; Morales-Lladosa, J.A. Location Problem in Relativistic Positioning: Relative Formulation. *Universe* **2024**, *10*. https://doi.org/10.3390/universe10070299.
13. Delva, P.; Kostić, U.; Čadež, A. Numerical modeling of a Global Navigation Satellite System in a general relativistic framework. *Advances in Space Research* **2011**, *47*, 370–379. Scientific applications of Galileo and other Global Navigation Satellite Systems - I, https://doi.org/https://doi.org/10.1016/j.asr.2010.07.007.
14. Kostić, U.; Horvat, M.; Gomboc, A. Relativistic Positioning System in perturbed spacetime. *Classical and Quantum Gravity* **2015**, *32*, 215004. https://doi.org/10.1088/0264-9381/32/21/215004.
15. Puchades, N.; Sáez, D. Approaches to relativistic positioning around Earth and error estimations. *Advances in Space Research* **2016**, *57*, 499–508. https://doi.org/https://doi.org/10.1016/j.asr.2015.10.031.

 doi:10.20944/preprints202604.0665.v1

16. Carloni, S.; Fatibene, L.; Ferraris, M.; McLenaghan, R.G.; Pinto, P. Discrete relativistic positioning systems. *General Relativity and Gravitation* **2020**, *52*, 12. https://doi.org/10.1007/s10714-020-2660-9.
17. Feng, J.C.; Hejda, F.; Carloni, S. Relativistic location algorithm in curved spacetime. *Phys. Rev. D* **2022**, *106*, 044034. https://doi.org/10.1103/PhysRevD.106.044034.
18. Coll, B.; Ferrando, J.J.; Morales, J.A. Two-dimensional approach to relativistic positioning systems. *Phys. Rev. D* **2006**, *73*, 084017. https://doi.org/10.1103/PhysRevD.73.084017.
19. Coll, B.; Ferrando, J.J.; Morales, J.A. Positioning with stationary emitters in a two-dimensional space-time. *Phys. Rev. D* **2006**, *74*, 104003. https://doi.org/10.1103/PhysRevD.74.104003.
20. Coll, B.; Ferrando, J.J.; Morales-Lladosa, J.A. Positioning in a flat two-dimensional space-time: The delay master equation. *Phys. Rev. D* **2010**, *82*, 084038. https://doi.org/10.1103/PhysRevD.82.084038.
21. Pozo, J. *Constructions in 3D (I) and (II)*; Talks delivered at the School on Relativistic Coordinates, Reference and Positioning Systems (University of Salamanca, Spain), 2005.
22. Ferrando, J.J.; Sáez, J.A. An intrinsic characterization of the Schwarzschild metric. *Classical and Quantum Gravity* **1998**, *15*, 1323. https://doi.org/10.1088/0264-9381/15/5/014.
23. Ferrando, J.J.; Sáez, J.A. An intrinsic characterization of the Kerr metric. *Classical and Quantum Gravity* **2009**, *26*, 075013. https://doi.org/10.1088/0264-9381/26/7/075013.
24. Ferrando, J.J.; Sáez, J.A. An intrinsic characterization of spherically symmetric spacetimes. *Classical and Quantum Gravity* **2010**, *27*, 205024. https://doi.org/10.1088/0264-9381/27/20/205024.
25. Mengual, S. Physical interpretation of spherically symmetric perfect fluid solutions to Einstein's equations, 2026, [arXiv:gr-qc/2512.19212].